Proceedings of NHTC '01
35th National Heat Transfer Conference
June 10-12, 2001, Anaheim, California, USA

NHTC 2001-20244

INTERNAL THERMAL MANAGEMENT FOR ELECTROCHEMICAL BATTERIES

R. J. Parise*
Parise Research Technologies

101 Wendover Road
Suffield, Connecticut 06078
Phone: (860) 668-4599

G. F. Jones
Department of Mechanical Engineering

Villanova University
Villanova, Pennsylvania 19085
Email: gerard.jones@villanova.edu

ABSTRACT

Secondary (rechargeable) electrochemical batteries provide a means for supplying electrical power to equipment. Thermal management is needed to reduce the temperatures caused by internal energy generation inside the batteries, a direct consequence of the chemical reactions required to produce the electrochemical potential. Depending on the electrolyte, anode and cathode materials, energy generation can occur during discharge, recharge, or both. For particular electrochemical battery systems, internal heat generation caused by I^2R losses can be considerable as well. Energy generation is a detriment to the operation of the battery, reducing life, increasing recharge time, and/or limiting output due to restricted discharge rates.

We consider a strategy for thermal management of rechargeable electrochemical batteries. The strategy consists of thermoelectric (TE) elements placed at the battery boundary connected to a heat conducting plate in contact with the energy-generating electrolyte region of the battery. Quasi-steady, two-dimensional analytical and numerical models have been developed for a Ni-Zn battery system. Ni-Zn batteries are susceptible to thermal build-up during excessive discharge; the increased temperatures cause damage to cell structure components. The models include heat generation due to the chemical reaction in the Ni-Zn cell, and heat transfer in the cold junction plate of the TE cooler in thermal contact with the electrolyte and the electrodes inside the battery. The thermal models provide the temperature distribution throughout the battery electrolyte region, as well as the temperature distribution in the cold-junction plate.

The results have shown that better internal thermal management in electrochemical batteries utilizing TE coolers will improve battery performance in the demanding applications required for the automotive industry and small battery-powered bicycles. In particular, the ratio of the discharge time for a TE-cooled Ni-Zn battery operating at a peak temperature of 332 K to that for a non-TE-cooled battery at the same peak temperature was calculated. The results showed that *TE cooling of the battery allows the discharge time to be reduced by more than a factor of two over that for an un-cooled battery.*

NOMENCLATURE

A area, m^2
d area density
E heat, J
I current, A
k thermal conductivity, W/m·K
K thermal conductance, W/K
ℓ length in y direction, m
L length in x direction, m
n number of TE modules
Q heat transfer rate, W
R electrical resistance, Ω
S Seebeck coefficient, V/K
t thickness, m
T temperature, K
w length normal to x and y, m
x coordinate, m

*Address all correspondence to this author.

y coordinate, m
α $|S_n| + |S_p|, V/K$
β coefficient of performance
γ aspect ratio, ℓ_e/L_e
Γ coefficient defined by eqn. (13)
λ coefficient defined by eqn. (15)
η $I_{TE}/I_{TE,max}$
ρ electrical resistivity, Ω·m
τ discharge time, min

Subscripts
b base case
C cold junction
e electrolyte
H hot junction
max maximum
n n junction
p p junction
q quadrant
s strip
TE thermoelectric
v variation
x x direction
y y direction

Superscript
$*$ no TE modules

INTRODUCTION

Secondary (rechargeable) electrochemical batteries provide a means for supplying electrical power to equipment. Thermal management is needed to control unwanted heat generation inside the batteries, a direct consequence of the chemical reactions required to produce the electrochemical potential. Depending on the electrolyte, anode and cathode materials, this heat generation can occur during discharge, recharge, or both. For particular electrochemical battery systems, internal heat generation caused by I^2R losses can be considerable as well.

Internal heat generation is a detriment to the operation of the battery, reducing life, increasing recharge time, and/or limiting output due to restricted discharge rates. Especially in the automotive industry and for small battery-powered bicycles, where traction batteries are required to power the vehicles, quick recharge and extreme loading on the battery system are typical during normal vehicle operation. This puts an excessive thermal load on the battery, greatly reducing performance and longevity. The physical size of the batteries limits the amount of heat that can be removed from external surfaces, causing a damaging heat buildup inside the battery and restricting operation.

There are several sources of heat generation in secondary batteries that result in thermal build-up (Crompton, 1997). Some are due to particular battery types or designs. However, there are two main causes inherent to all batteries. One is electrical I^2R losses during discharge or recharging. Quick recharge times requiring high charging rates can result in very large losses. Typically, with the resulting thermal build-up in the battery, charging must be interrupted to allow the heat to dissipate, extending recharge time.

The second source of thermal energy in electrochemical batteries are the various reactions that take place during both discharge and charging. For example, in lead-acid batteries the chemical reaction that produces the electromotive force, lead and lead dioxide with sulfuric acid, causes an exothermic heating of the battery. During charging, this is an endothermic reaction that actually cools the battery. However, during typical recharge rates, the I^2R losses more than offset this cooling, resulting in a net increase in thermal energy. And for very high charging rates, the cooling effect becomes insignificant.

Thus, the primary source of heat production occurs in the metal grid plates, both at their surface where the chemical reactions take place and internally where the current flows and the electrical resistance causes the heat generation. The heat generated in the battery is difficult to remove since this location is not easily accessible. Thus, the bulk and configuration of large batteries do not lend themselves to cooling strategies. Nonetheless, if cooling can be provided at the point of this heat generation, improved recharge times and battery performance will result. The application of thermoelectric (TE) coolers at the source of heat production will aid in battery longevity and increase practical usage of the battery. The coolers may be positioned in any or all of several locations internal to the battery for the best results of heat removal. Several different configurations for TE cooling were proposed in an earlier paper (Parise, 2000).

One of these strategies has the TE coolers installed between the positive and negative grid plates of the cell pairs (see Fig. 1). Construction has to be such that the electrolyte can still flow easily between the plates during both discharge and recharge of the battery. With this strategy, the coolers are in good thermal contact with the prime source of heat production, the metal grid plates. The cold junction plate appearing in Fig. 1 is a good heat-conducting rectangular ring or strip that allows the free flow of electrolyte between the grid pairs. The air-cooled, warm junctions of the TE modules are on the exterior of the battery.

Under certain operating conditions, the interior of the battery may require heating. In this application, current flow can be reversed in the TE modules to control the battery internal temperature. Obviously, control circuitry would be needed to maintain a specified temperature.

In this paper, two-dimensional, analytical and numerical models have been developed to predict the thermal performance of a Ni-Zn battery system. Ni-Zn batteries are susceptible to thermal build-up during excessive discharge; the increased temperatures cause damage to cell structure components. The models

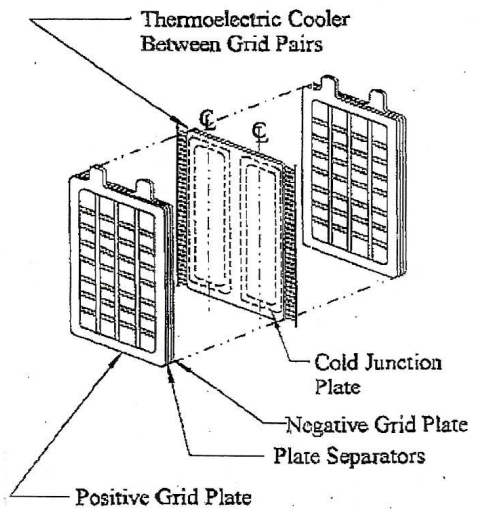

Figure 1. SCHEMATIC OF THE COLD JUNCTION PLATE PLACED BETWEEN PLATE PAIRS IN THE BATTERY.

include heat generation due to the chemical reaction in the Ni-Zn cell, $2\mathrm{NiOH(OH)} + \mathrm{Zn} + 2\mathrm{H} \rightarrow 2\mathrm{Ni(OH)} + \mathrm{Zn(OH)}$, and conduction in the cold junction plate of the thermoelectric cooler in thermal contact with the electrolyte and the electrodes inside the battery. The models provide the temperature distribution throughout the battery electrolyte region, as well as the temperature distribution in the cold junction plate.

MODELING

The Governing Equations

We consider quasi-steady, two-dimensional conduction in a rectangular cell of a battery bounded by a cold-junction plate which we model as a conducting strip. One quadrant of the cell appears as shown in Fig. 2. The cell dimensions are $2L_e$ in the x direction, $2\ell_e$ in the y direction, and w_e thick. There is a quasi-steady, uniform energy generation rate per unit volume which results in a heat transfer rate Q_q at the boundary of the cell. Thermoelectric (TE) coolers in the form of a number, n, of TE modules are installed on the vertical side of the quadrant with the cold side (at temperature $T_C(y)$), in intimate contact with the strip and the hot side at constant temperature T_H.

The temperature distribution in the electrolyte, $T_e(x,y)$, for

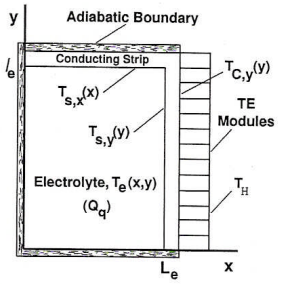

Figure 2. CROSS SECTION OF A QUADRANT OF A BATTERY CELL FOR USE IN FORMULATING THE THERMAL MODEL.

$0 \le x \le L_e$ and $0 \le y \le \ell_e$ is governed by the heat conduction equation

$$\frac{\partial^2 T_e}{\partial x^2} + \frac{\partial^2 T_e}{\partial y^2} + \frac{Q_q}{L_e \ell_e w_e k_e} = 0, \tag{1}$$

The outer surface of the strip is insulated at the terminal-side (i.e., top) of the battery, and has TE modules installed on the vertical side. The strip has a thickness t_s, width w_{TE}, and thermal conductivity k_s. The temperature distribution in the strip is from the solution of

$$k_s t_s w_{TE} \frac{d^2 T_{s,x}}{dx^2} - k_e w_e \left.\frac{\partial T_e}{\partial y}\right|_{y=\ell_e} = 0, \tag{2}$$

along the top side of the battery, and

$$\frac{k_s t_s w_{TE}}{w_e} \frac{d^2 T_{s,y}}{dy^2} - k_e \left.\frac{\partial T_e}{\partial x}\right|_{x=L_e} - \frac{Q_{TE}(y)}{A_{TE}} = 0, \tag{3}$$

along the vertical side. $Q_{TE}(y)$ is the local heat transfer rate at the cold junction of a TE module, A_{TE} the cross-sectional area for a TE module normal to the vertical side, and w_e and k_e are the thickness and thermal conductivity of the electrolyte, respectively.

The boundary conditions are

$$\left.\frac{\partial T_e}{\partial x}\right|_{x=0} = \left.\frac{\partial T_e}{\partial y}\right|_{y=0} = \left.\frac{dT_{s,x}}{dx}\right|_{x=0} = \left.\frac{dT_{s,y}}{dy}\right|_{y=0} = 0, \tag{4}$$

along the battery centerlines, and a match between the strip and battery temperatures where the two meet. Thus,

$$T_e(x, y=\ell_e) = T_{s,x}(x), \qquad 0 \le x \le L_e, \tag{5}$$

and

$$T_e(x=L_e, y) = T_{s,y}(y), \qquad 0 \le y \le \ell_e, \tag{6}$$

along with

$$T_{s,y}(y=\ell_e) = T_{s,x}(x=L_e). \quad (7)$$

$Q_{TE}(y)$ is from an energy balance on a TE module which includes heat transfer from the Seebeck effect less the parasitic heat transfer from both electrical resistance heating and conduction from the surroundings. We have (Angrist, 1982),

$$Q_{TE}(y) = \alpha T_{C,y}(y) I_{TE} - I_{TE}^2 R_{TE}/2 - K_{TE}[T_H - T_{C,y}(y)], \quad (8)$$

where $\alpha = |S_n| + |S_p|$, and R_{TE} and K_{TE} are the electrical resistance and thermal conductance of a TE module expressed as follows

$$R_{TE} = \rho_n L_n/A_n + \rho_p L_p/A_n, \quad K_{TE} = k_n A_n/L_n + k_p A_p/L_p. \quad (9)$$

$T_{C,y}(y), T_H$, and I_{TE} are the cold- and hot-junction temperatures of the module, and module current, respectively.

As we discuss below, it will be convenient to consider the situation for a uniform cold-junction temperature, T_C. In this case, the current required to maximize the heat transfer rate at the cold junction of a TE module is determined by setting the derivative of eqn. (8) with respect to I_{TE} equal to zero and solving for $I_{TE} = I_{TE,max}$. Obtain,

$$I_{TE,max} = \frac{\alpha T_C}{R_{TE}}. \quad (10)$$

If we define η as the ratio of actual current supplied to the TE modules to $I_{TE,max}$,

$$\eta = \frac{I_{TE}}{I_{TE,max}}, \quad (11)$$

eqn. (8) can then be solved for the ratio of T_C to T_H and written as

$$\frac{T_C}{T_H} = \Gamma[-1 + \sqrt{1 + \frac{2}{\Gamma}(1 + \frac{Q_q}{n T_H K_{TE}})}], \quad (12)$$

where Γ is from

$$\Gamma = \frac{R_{TE} K_{TE}}{\alpha^2 \eta (2-\eta) T_H}. \quad (13)$$

Thus, we see by inspecting eqs. (12) and (13), that T_C is calculable for known values of T_H, the dimensions and properties for a TE module, and specified values for the fraction of the maximum current, η, and the heat transfer rate per module at the cold junction, Q_q/n. Use will be made of eqn. (12) below.

Numerical Approach and Results

Equations (1)-(9) were solved numerically by writing eqs. (1)-(3) and the associated boundary conditions in finite-difference form on a uniform grid. All derivatives were approximated using second-order accurate differences. The resulting system of non-linear algebraic equations was solved by iteration and relaxation using MATLAB. We found that the results were independent of the mesh size for a grid of 21 by 21 nodes in each direction. A relative convergence criterion of better than 0.001 was used for the temperature at each node. About 800-1000 iterations were required to achieve convergence.

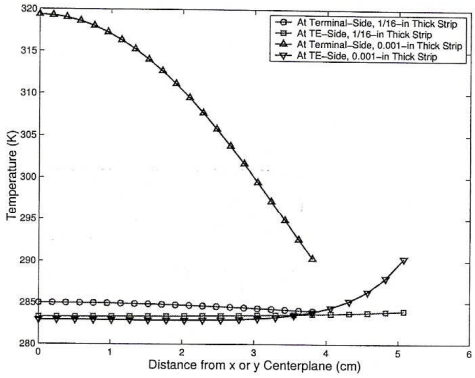

Figure 3. TEMPERATURE DISTRIBUTION ALONG EDGES OF A CELL IN THE BATTERY. FROM NUMERICAL SOLUTION.

Of particular interest from the results of the numerical solution is the sensitivity of the results to the conductance of the conducting strip. In Fig. 3, we show the temperature distribution for an aluminum strip having the thickness values of 0.00254 cm (0.001 in) (essential zero thickness), and 0.318 cm (1/16 in). The values for γ, Q_q, and η are set equal to their respective base-case values discussed below.

It is clear from our inspection of Fig. 3 that a strip thickness of 0.318 cm (1/16 in) or more is sufficient to produce a near uniform (say, better than 2%) temperature distribution at the boundary of the battery. An increase in the strip thickness to twice this value resulted in a maximal temperature variation along the length of the strip of less than 1 K.

A plot of the temperature distribution in the quadrant of the battery for the base case is shown in Fig. 4. We note that the peak temperature of the battery occurs at the battery center and is about 332 K.

Analytical Approach

As discussed above, the temperature at the boundary of the battery is uniform at T_C for a sufficiently thick conducting strip. The temperature distribution in the battery, T_e, can then be written as (Arpaci, 1966)

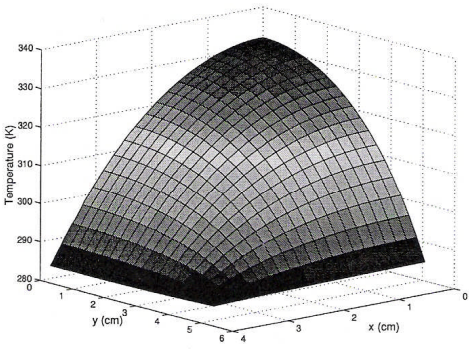

Figure 4. TEMPERATURE DISTRIBUTION IN A CELL OF THE BATTERY. FROM NUMERICAL SOLUTION.

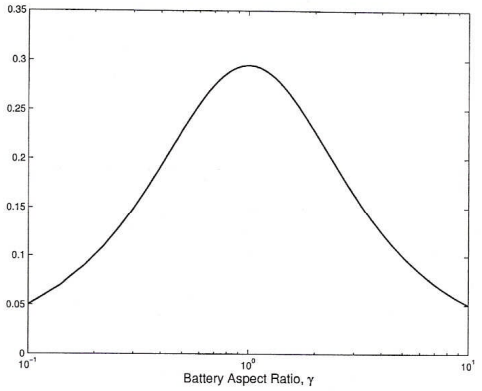

Figure 5. THE FUNCTION $\phi(\gamma)/\gamma$.

$$\frac{T_e(x,y)-T_C}{Q_q/(w_e k_e \gamma)} = \frac{1-(x/L_e)^2}{2} - 2\sum_{m=0}^{\infty} \frac{(-1)^m}{\lambda_m^3} \frac{\cosh(\lambda_m y/L_e)}{\cosh(\lambda_m \gamma)} \cos(\lambda_m x/L_e), \tag{14}$$

where

$$\lambda_m = (m+\frac{1}{2})\pi, \quad \gamma = \frac{\ell_e}{L_e}. \tag{15}$$

The maximum temperature, $T_{e,max}$, occurs at the center of the battery. Thus, we can write

$$\frac{T_{e,max}-T_C}{Q_q/(w_e k_e \gamma)} \equiv \phi(\gamma) = \frac{1}{2} - 2\sum_{m=0}^{\infty} \frac{(-1)^m}{\lambda_m^3 \cosh(\lambda_m \gamma)}. \tag{16}$$

Equations (12) and (16) can be combined to obtain an expression for the maximum temperature in the battery relative to T_H

$$\frac{T_{e,max}}{T_H} = \Gamma[-1+\sqrt{1+\frac{2}{\Gamma}(1+\frac{Q_q}{n T_H K_{TE}})}] + \frac{Q_q}{w_e k_e T_H} \frac{\phi(\gamma)}{\gamma}. \tag{17}$$

The first term on the RHS of eqn. (17) accounts for the difference in temperature between T_H and T_C across the TE modules, and the second term, for the difference in temperature between the center of the battery and T_C. As seen in Fig. 5, the function $\phi(\gamma)/\gamma$ is a maximum of 0.281 at γ of 1 and decreases for larger and smaller values of γ. Since a reduction or an increase in γ places one of the TE-cooled boundaries closer to the center of the battery, the maximum battery temperature decreases with a departure of γ from unity in either direction.

With no TE modules attached to the battery, $T_C = T_H$, and eqn. (17) becomes

$$\frac{T^*_{e,max}}{T_H} = 1 + \frac{Q_q}{w_e k_e T_H} \frac{\phi(\gamma)}{\gamma}. \tag{18}$$

THE DATA

We have obtained limited data (Cao, et al., 2000; Cao, 2001) for a 30 A-h, Ni-Zn battery of cross-sectional dimensions $2\ell_e$ of 10.2 cm (4 in) high by $2L_e$ of 7.62 cm (3 in) wide. Thus, γ_b is 1.33. In the battery there are 7 cells, each having 20 plate pairs. Each plate pair is separated by an electrolyte of proprietary composition and thickness w_e of 0.038 cm (0.015 in). The thermal conductivity of the electrolyte is about 75% of that of water and calorimetry tests on the battery during discharge have shown a release of 8.4 kJ of heat in a 3-h period. The heat release over the discharge period is calculated as 63 J/quadrant for a plate pair in the battery.

Additional heat release data may be obtained by assuming a conversion efficiency of 85% for a battery which possesses a conventionally accepted energy density of 95 W-h/ℓ (Crompton, 1997; Cao, 2001). These data result in a heat release of 39 J/quadrant for a plate pair. With these two data sets, we may estimate the quasi-steady heat transfer rate from the quadrant of the battery, Q_q, as

$$Q_q = \frac{\{[(63+39)\pm(63-39)]/2\}\text{J}}{\tau} = \frac{E_b \pm E_v}{\tau}, \tag{19}$$

where $E_b = 51$ J (the base case), $E_v = 12$ J, and τ is the discharge time.

In the results that follow, the plate area for the battery, A_q, and battery volume will be held constant for the sake of consistency in the comparisons that appear below. Thus, we may write

$$L_e = \sqrt{A_q/\gamma}, \quad \ell_e = \sqrt{A_q \gamma}, \tag{20}$$

where $A_q = (10.2 \times 7.62)/4$ cm^2.

RESULTS AND DISCUSSION

The Parameters

An inspection of the above equations shows that the following four dimensionless groups determine the maximum battery temperature ratio, $T_{e,max}/T_H$: $\Gamma, Q_q/(w_e k_e T_H), Q_q/(nT_H K_{TE})$, and γ. In this section, we choose the base-case values for several of the parameters in these groups. Key among these parameters are the aspect ratio, γ, current ratio, η, and the heat flow rate, Q_q.

The base-case value for T_H is held constant at 313 K to correspond to battery usage in warm environments (Cao, et al., 2000). The parameters n and Γ are determined by the battery geometry, as well as the selection of the type of TE element. We consider bismuth-telluride TE elements, each 1 mm by 1 mm ($=w_{TE}$) in cross section and 2.54 cm long for which the following data apply: $S_n = -199 \times 10^{-6}$ V/K, $S_p = 202 \times 10^{-6}$ V/K, $\rho_n = 0.9813 \times 10^{-5}$ Ω·m, $\rho_p = 1.0702 \times 10^{-5}$ Ω·m, and $k_n = k_p = 1.5$ W/m·K. We assume a total of 0.5 mm of distance between consecutive TE modules (an area density for the modules, d_{TE}, of 0.8) so that the number of modules may be written as

$$n = \frac{\ell_e d_{TE}}{2 w_{TE}}. \tag{21}$$

The base-case value for n is about 20.

The base-case value for η is chosen such that, when combined with T_H from above and E_b from eqn. (19), the value for T_C will satisfy the following. First, from the standpoint of practical considerations, T_C should obviously be above the local dew point temperature. Second, we consider that the Ni-Zn cell performs optimally when it is in the temperature range of 298-301 K (Falk and Salkind, 1969). Given the relatively small value for the thermal conductivity of the electrolyte, and thus the associated large value for the temperature gradient through it, we arbitrarily select a base-case value for T_C of 283 K. Through eqn. (12), E_b, γ, eqn. (21), and the above properties, T_C of 283 K produces a base-case value for η of about 0.23.

The Results

The maximum battery temperature as a function of the discharge time appears in Figs. 6 (without TE cooling) and 7 (with TE cooling). In each case, as the discharge time increases, the reduction in the energy generation rate results in a lowering of the peak battery temperature. The maximum useful battery temperature of 332 K (Cao, et al., 2000) is shown on each of these figures. For peak temperatures greater than 332 K, battery performance decreases sharply.

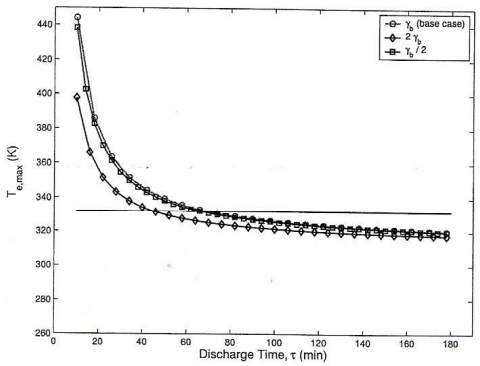

Figure 6. MAXIMUM BATTERY TEMPERATURE VS. DISCHARGE TIME AND ASPECT RATIO, γ, WITHOUT TE MODULES. MAXIMUM BATTERY TEMPERATURE OF 332 K IS SHOWN.

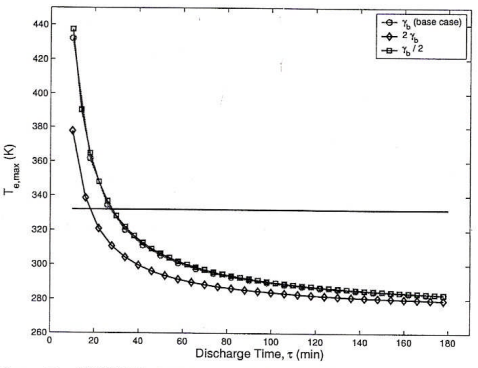

Figure 7. MAXIMUM BATTERY TEMPERATURE VS. DISCHARGE TIME AND ASPECT RATIO, γ, WITH TE MODULES. MAXIMUM BATTERY TEMPERATURE OF 332 K IS SHOWN.

It is more enlightening to compare the relative reduction in discharge time due to TE cooling of the battery. This is presented in Fig. 8 where we show the ratio of the discharge time for a TE-cooled battery operating at a peak temperature of 332 K to that for a non-TE-cooled battery at the same peak temperature. The results are calculated as a function of the current ratio, η, for

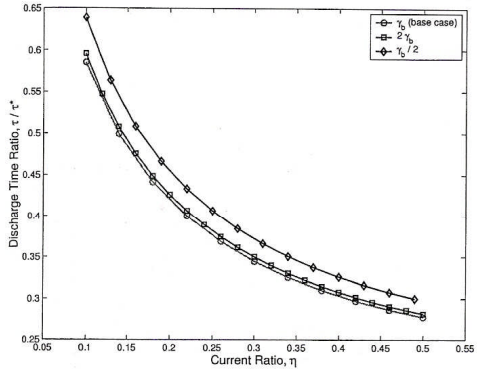

Figure 8. DISCHARGE TIME RATIO WITH TE MODULES VS. WITHOUT TE MODULES TO PRODUCE A MAXIMUM BATTERY TEMPERATURE OF 332 K. THREE VALUES OF ASPECT RATIO, γ, SHOWN.

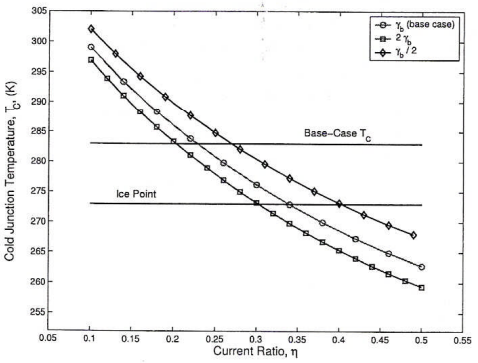

Figure 9. COLD JUNCTION TEMPERATURE, T_C VS. CURRENT RATIO, η, AND ASPECT RATIO, γ.

three values of the aspect ratio, γ. From inspection of this figure, it is clear that TE cooling of the battery allows the discharge time to be reduced by more than a factor of two. In fact, for the base case value of η, the ratio of the discharge times is about 0.4.

However, the reduction in discharge time comes with a lowering of the temperature at the outside surface of the battery. Thus, attention must be given to Fig. 9 to ensure that a value for η is chosen that will produce an acceptable value for T_C. With TE cooling, the discharge time for the base case is about 28 min which produces a base-case value for Q_q of 0.0320 W. For the

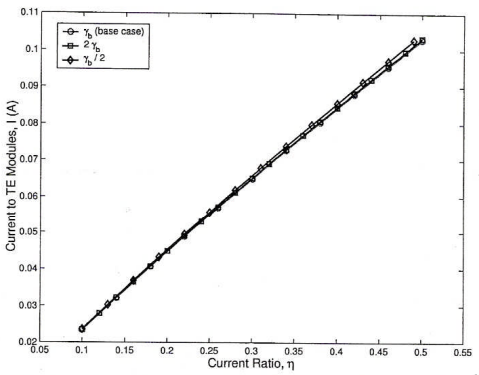

Figure 10. CURRENT TO TE MODULES VS. CURRENT RATIO, η, AND ASPECT RATIO, γ.

higher value of the energy dissipation of 63 J, the discharge time is about 33 min. Both cases assume a constant battery temperature of 332 K during discharge so that Q_q is the same for each.

The current to the TE modules, shown in Fig. 10, is used to calculate the required TE electrical power and coefficient of performance, β (Fig. 11). The slight non-linear variation in I_{TE} with η evident in Fig. 10 is due to the influence of T_C which also varies with η (see eqs. (10)-(11)).

The COP, β, calculated from

$$\beta = \frac{Q_q}{(\eta I_{TE,max})^2 R_{TE} n}, \tag{22}$$

is seen to range from 5 at the smallest value of η to slightly less than 1 for the largest (Fig. 11). There is only a weak sensitivity of β with γ as shown in Fig. 11. The reciprocal of β, the ratio of the electrical power to the TE modules to the heat transfer rate, thus spans from 0.20 to about one. However, for a nominal battery efficiency of 85%, the ratio of electrical power to the TE modules to the electrical power output of the battery is calculated to be less than 15%.

The influence of aspect ratio, γ, on maximum battery temperature arises solely from the change in the internal thermal resistance between the battery center and the cooled boundary as the aspect ratio is changed. This effect is manifested by the term $\phi(\gamma)/\gamma$ in eqs. (17)-(18). For γ of γ_b, $2\gamma_b$, and $\gamma_b/2$ (1.33, 2.66, and 0.667; γ_b and $\gamma_b/2$ are both relatively close to one) the values for $\phi(\gamma)/\gamma$ are 0.281, 0.182, and 0.269, respectively. Thus, the small difference between $\phi(\gamma_b)/\gamma_b$ and $\phi(\gamma_b/2)/(\gamma_b/2)$ causes only small differences in the results for these two cases appearing in Figs. 6-8 above.

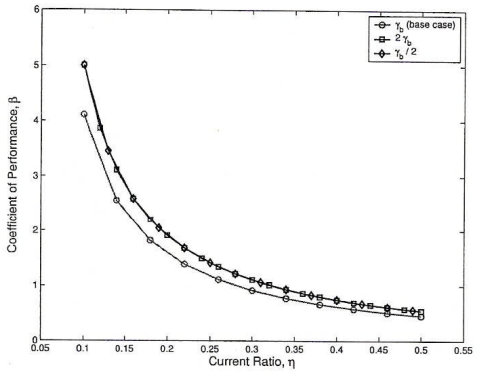

Figure 11. COEFFICIENT OF PERFORMANCE FOR TE MODULES, β, VS. CURRENT RATIO, η, AND ASPECT RATIO, γ.

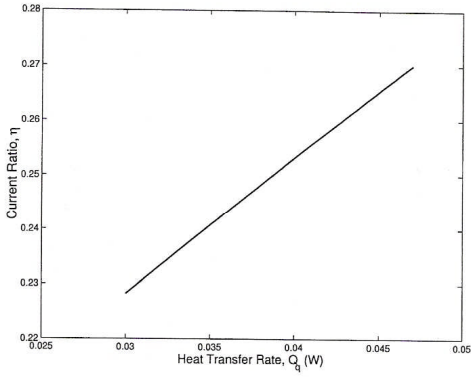

Figure 12. CURRENT RATIO, η, VS. HEAT TRANSFER RATE, Q_q, FOR T_C= 283 K.

The dependence of T_C on γ as seen in Fig. 9 may be explained by the following. The heat transfer rate from a quadrant of a cell is relatively small (of the order of 0.03 W) so that, in general,

$$\frac{Q_q}{n T_H K_{TE}} \ll 1, \tag{23}$$

and we are able to write eqn. (12) as,

$$\frac{T_C}{T_H} \approx a + b \frac{Q_q}{n T_H K_{TE}}, \tag{24}$$

where a and b are constants. Therefore, for a fixed value of Q_q, T_C is inversely proportional to n through eqn. (24). An increase in γ causes an increase in ℓ_e (through eqn. (20)), a subsequent increase in n (through eqn. (21)), and by eqn. (24), a decrease in T_C. Our inspection of Fig. 9 confirms this trend. Thus, T_C is inversely proportional to n, γ, and ℓ_e, and directly proportional to Q_q.

The effects of an increase in heat release from the battery during discharge are addressed next. We will consider the influence of the release of 63 J of energy over the discharge time of 28 min which produces 0.0375 W of thermal power dissipated in one quadrant of a battery cell.

The basic assumption underlying Fig. 8 is that the peak battery temperature is fixed at 332 K. Thus, the heat flow rate through the boundary of the battery, and the results appearing in Fig. 8, are the same independent of the value of the heat release. Therefore, the conclusions drawn above concerning Fig. 8 are unchanged for the larger dissipation rate.

The effect of Q_q on η is the focus of Fig. 12. In Fig. 12, we plot the current ratio, η, as a function of the heat transfer rate, Q_q, for a fixed cold plate temperature of 283 K. From our inspection of Fig. 12 for Q_q of 0.0375 W, the value for η increases to 0.25 from the base-case value of 0.23. The value for the current, I_{TE}, increases 0.02/0.23, or about 9%.

Equation (22) shows that β is a function of Q_q/η^2. Thus, since η depends linearly on Q_q (Fig. 12), then β is inversely proportional to Q_q. For Q_q of 0.0375 W, β is about 24% less than its base-case value.

CONCLUSIONS

A strategy for the internal thermal management of electrochemical batteries was considered in this work. The strategy utilizes thermoelectric (TE) coolers and a heat conducting strip or cold plate in contact with the energy-generating components of the battery. The results have shown that better internal thermal management in electrochemical batteries utilizing TE coolers will improve battery performance in the demanding applications required for the automotive industry and small battery-powered bicycles.

Quasi-steady, two-dimensional, numerical and analytical models were produced and an investigation of the effects of several key parameters on the performance of a Ni-Zn battery was undertaken. Among the salient results from this study are the following:

1. For the range of heat transfer rates from the battery considered in this work, a conducting strip thickness of 0.318 cm (1/16 in) or more is sufficient to produce a near uniform (say, better than 2%) temperature distribution at the boundary of the battery.

2. The ratio of the discharge time for a TE-cooled battery operating at a peak temperature of 332 K to that for a non-TE-cooled battery at the same temperature was calculated. The results showed that *TE cooling of the battery allows the discharge time to be reduced by more than a factor of two over that for an un-cooled battery.*
3. A cold junction temperature, T_C, of 283 K is chosen by considering the optimal mean operating temperature of the battery and the practical constraint that T_C be above the local dew point temperature.
4. Since T_C is specified as described above, the heat transfer rate from the battery determines the:
   (a) Current, and thus electrical power, to the TE modules through eqn. (12),
   (b) Peak battery temperature through eqn. (17),
   (c) Coefficient of performance of the TE modules through eqn. (22).
5. The influence of battery aspect ratio on maximum battery temperature arises solely from the internal thermal resistance between the battery center and the cooled boundary. In particular, this thermal resistance is a maximum for aspect ratio of one, and reduces for aspect ratios either less, or greater, than one.
6. The TE modules require less than 15% of the electrical power output of the battery and operate with a coefficient of performance of approximately one.

FUTURE WORK

The next part of this work will address the transient performance of the battery. In most cases, the battery load is inherently time dependent, i.e., I_{TE} is a function of time. In addition, the energy generated within the battery becomes time-dependent through the resulting time-dependent electrolyte temperature. Among the cases that will be considered in this phase, we will address the battery performance under conditions of repeated short-term, peak-power demand each followed by a cooling period.

ACKNOWLEDGMENT

The authors gratefully acknowledge the inspiration of R. Joseph Parise, Jr., during the research phase of this paper. His valiant efforts in sustaining life were the driving force in the final preparation of this manuscript.

REFERENCES

Angrist, S. W., 1982, *Direct Energy Conversion*, 4th Ed., Allyn and Bacon, Boston, MA.

Arpaci, V. S., 1966 *Conduction Heat Transfer*, Addison-Wesley, Reading, MA.

Cao, F., Charkey, A. and Williams, K., 2000, "Thermal Behavior and End-Of-Life Characteristics of the Nickel-Zinc Battery," Paper AIAA-2000-2975, *Proc. IECEC 2000*, Las Vegas, NV.

Cao, F., 2001, Personal Communication.

Falk, S. U. and Salkind, A. J., 1969, *Alkaline Storage Batteries*, Wiley, New York, NY.

Parise, R. J., 2000, "Quick Charge Battery with Internal Thermal Management," Paper AIAA-2000-2818, *Proc. IECEC 2000*, Las Vegas, NV.